International Journal of Robotics and Control Systems
Vol. 4, No. 1, 2024, pp. 291-311
ISSN 2775-2658
http://pubs2.ascee.org/index.php/ijrcs

Analysis of Drone Wireless Communication System Performance Affected by Vibration based on 1DCNN

Ahmed Hussein Abbas [a,1], Hassanain Ghani Hameed [b,2], Ahmad Taha Abdulsadda [b,3]

a Department of Communication Technical Engineering, Al-Furat Al-Awsat Technical University, Al Najaf, 540001, Iraq
b Engineering Technical College/ Najaf, Al-Furat Al-Awsat Technical University, Al Najaf, 540001, Iraq
[1] ahmed.ms.etcn39@student.atu.edu.iq; [2] hassanain.hameed@atu.edu.iq; [3] coj.abdulsad@atu.edu.iq

ARTICLE INFO

Article history
Received January 11, 2024
Revised March 09, 2024
Accepted March 18, 2024

Keywords
Drone Vibrations;
Vibration Analysis;
Symbol Error Rate (SER);
1DCNN;
Monte-Carlo

ABSTRACT

Developments in drone technology have made them crucial in various fields. Vibrations caused by external conditions or mechanical failures in a drone's design can significantly affect the efficiency of the drone's communication systems. The drone's antenna generates phase noise, which can degrade the performance of drone communications systems. This work presents an analysis and computational model of how drone vibration affects system performance. by using two steps. The first one uses the simulation Monte-Carlo in MATLAB when the iteration algorithm processes with various variable values as the frequency carriers and the order of the quadrature-amplitude-modulation (M-QAM) system and evaluates the performance of the communication system by measuring the symbol error rate. The second step uses the one-dimensional convolutional neural network to predict the symbol error rate. After creating the dataset in the first stage, reprocess it and split it into 70% training and 30% testing. Then, by MATLAB App Designer created a graphical user interface (GUI) for friendly use. The result appears to be that the performance of the drone communication system decreased when frequency carriers and modulation order for M-QAM increased due to the impact of a vibrating antenna. Our contribution to this work is using 1DCNN, unlike other works that only use simulation to evaluate the performance, because 1DCNN can automatically extract useful features from the input dataset to evaluate the effect. This study provides a valuable method to evaluate the efficiency of a communication system on the UAV, which is particularly important for drone wireless system planning. In our next work, we propose investigating other factors affecting UAV communication systems, including humidity and temperature.

1. Introduction

An unmanned aerial vehicle (UAV), commonly known as a drone have become more essential and used for different applications. Such activities as monitoring, environmental management, and civil security control require efficient safety procedures [1]. The two primary types of UAVs are fixed-wing and rotorcraft. In 2020–2022, fixed-wing UAVs with vertical takeoff and landing

(VTOL) capabilities developed rapidly [2]-[4]. Using electric or hybrid propulsion, combine Aeroplan and multirotor UAV capabilities [5]-[7]. Most UAVs are often supported by an onboard autopilot based on tiny sensors such as accelerometers, gyroscopes, barometers, and GPS. Precise estimation of a UAV's attitude and position is the first step towards precise machine control [8].

Fig. 1. Depicts the generic receiver and transmitter for control and video signal in the drone's communication system. Various conditions, such as weather, obstacles, distance, metal interference, radio interference, and frequency interference, impact a drone's signal transmission. Rain and heat can impact signal propagation, drone electronics, and batteries [9]. A crucial element is signal strength. In addition, the drone may move erratically and lose signal strength due to mechanical problems or wind vibrations. The system's primary beam direction, side lobes, and beam breadth change due to equivalent antenna movements caused by drone vibrations. Ultimately, these modifications may weaken the communication channel [10]-[13].

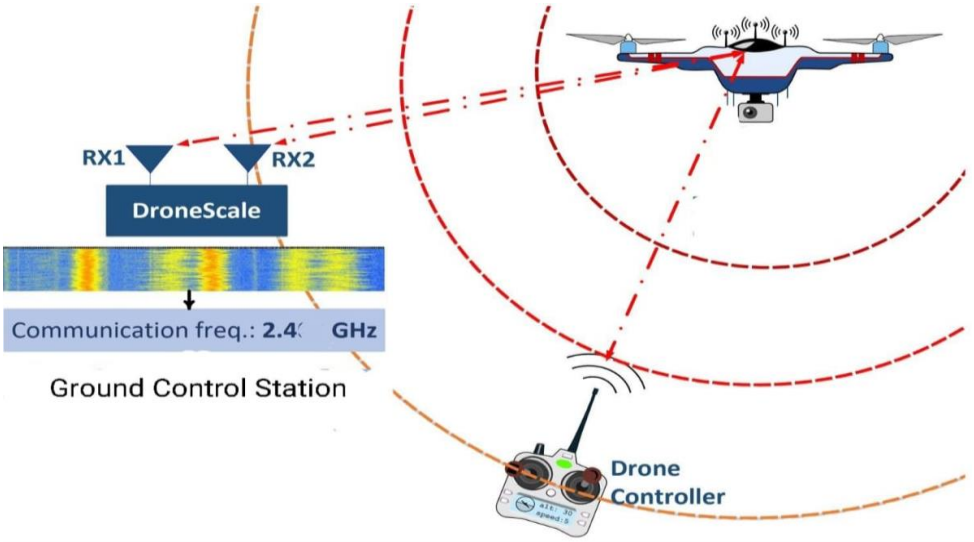

Fig. 1. General receiver and transmitter system for drone

Many scholars have been examined the primary vibration sources influencing this UAV and offered a computational and experimental vibration analysis of a multirotor chassis. The outcome data was used to do a numerical modal analysis of the UAV chassis, making it possible to identify low-vibration areas ideal for mounting sensitive electronics [14]. Investigated how the quality factor of the laser communication link in the optical inter-satellite network (OISN) system is affected by pointing mistakes brought on by vibrations in the satellite platform. This study also provides optimal laser power and wavelength specifications [15]. Looked at the possibility of analyzing vibration measurements from various flights to determine the state of the drone's internal components. The findings could help safety operators determine whether vibration anomalies in drone flights signal a severe problem progressing and serve as a diagnostic or troubleshooting tool [16]. Studied the effects of a variable 3-dimensional (3D) antenna beamwidth on a cellular network supported by unmanned aerial vehicles (UAVs).

Additionally, they examined the performance of typical user equipment (T-UE), paying particular attention to coverage probability and spectral efficiency (SE) when 3D antenna beamwidth fluctuations were present. The study highlights the significant disruption caused by antenna fluctuations [17]. And proposes a direct air-to-ground radio communication technique for rotary-wing UAVs that account for propellers. The model is utilized to present the investigation and its discoveries. The results indicate potential risks linked to adapting to the existing communication system and that the maximum Doppler shifts occur for all simulated frequencies over the LTE-required threshold of 300 Hz [18]. Studied the impact of UAV wobbling on the coherence time of

the wireless channel between UAVs and terrestrial user equipment (UE) using a Rician multipath channel model. The results of this study indicate that the channel's coherence time may degrade quickly, even for small wobbling UAVs. This could pose difficulties in tracking the channel and establishing a reliable communication link [19].

Many scholars have been conducted on the effects of antenna vibration, particularly on large reflector antennas [20]-[23]. Research has shown that the distortion of an antenna caused by vibration alters the radiation characteristics, including the radiation pattern, primary beam orientation, and beam breadth. Antenna vibration may increase measurement error, perhaps resulting in inaccurate estimates of the direction of arrival, as discussed in [24]. Furthermore, paired echo resulting from antenna vibration will significantly impact the picture quality of geosynchronous synthetic aperture radar [25]. The study also examined the impact of antenna vibration on phase noise. In reference [26]. Equations were derived to calculate phase noise based on vibration factors, and these equations were then validated using measurements. The transmitted signal's spectrum has substantial material beyond the fundamental frequency of vibration due to the chaotic oscillations of the antenna [27]. Focused their attention on investigating the effects of these vibrations on antennas and communications, as in [28]-[30]. Investigated the effects of antenna vibration in high-frequency (30 GHz) wireless communication systems. They examined the influence on SER for different values of SNR in BPSK, QPSK, and MQAM scenarios [31].

In this work, we study drone vibrations that produce phase noise and how phase noise affects the drone communication system, which can negatively impact the operation of wireless communication systems, using two methods. The first stage uses the simulation Monte Carlo in MatLab2021b when the iteration algorithm processes with various variable values as the frequency carriers (2.4 GHz, 5.8 GHz) and the order of the M-QAM system (4-QAM, 16-QAM, 32-QAM, or 64-QAM) and evaluates the performance of the communication system on the drone by measuring the symbol error rate SER. The second stage uses the convolutional neural network CNN to predict the symbol error rate (SER). After training and testing our model on the dataset that is created in simulation, the MATLAB App Designer creates a GUI that is easy and friendly for the user. Our contribution to this work is using 1DCNN, unlike other works that only use simulation to evaluate the performance of the unmanned aerial vehicle UAV communication system. This study provides a valuable method to evaluate the efficiency of a communication system on the UAV. We notice how degrading the drone communication system's performance is when we increase the carrier frequency and use high-order M-QAM. This is conducted to assess the influence of vibration on different conditions and to quantify the symbol error rate (SER).

This study is as follows: Section One provides an introductory literature survey and explains the methods used. Next, analyze the mathematical representation of antenna vibration within the framework of M-QAM in Section Two. Section three explains the theoretical background of the phase noise effect on communication systems and convolutional neural network (CNN) layers. Then, the methods used and explained the steps and algorithm to experiment with the vibration drone through the utilization of MATLAB 2021b in simulation Monte Carlo and convolution neural network CNN, specifically examining two frequencies, 2.4 GHz and 5.8 GHz, and different M-QAM, are outlined in Section Four. Section Five shows the results of the symbol error rate (SER).

Indifferent vibration and carrier frequencies. Signal-to-noise ratio (SNR) values using the Monte Carlo technique, CNN.Section six shows the discussion and The last section concludes with a thorough discussion and recommendations based on the results.

2. Mathematical Model

Vibrating antennas introduce Phase noise into transmissions, both in transmitting and receiving signals. When operating in high-vibration situations, microwave and millimetre-wave systems that demand low-phase noise at small frequency offsets must consider this noise source. The vibration may

be sinusoidal or random vibration. Let us assume that an oscillator produces a pure sine tone at frequency. Additionally, vibration does not affect this oscillator. An antenna, called antenna A, receives input from the oscillator. At a frequency, Antenna A is oscillating around the origin of the coordinate system. The vibrating antenna sends signals to a second antenna, known as antenna B, shown in Fig. 2. Antenna B is not vibrating; it is stationary.

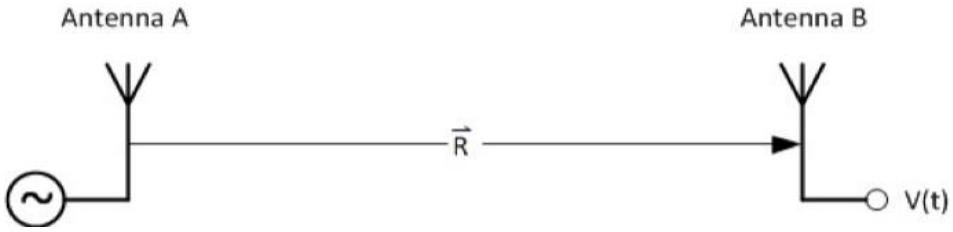

Fig. 2. Vibration from antenna A causes phase noise on antenna B's signal

Vibrating antennas derived by [20] introduce phase noise into transmissions. The position of Antenna A as a function of time.

$$\vec{x}(t) = \overrightarrow{x_o} sin\,(2\pi f_v t) \tag{1}$$

Increases the phase radiation with time by antenna A, and the slope is constant and equivalent to angular frequency. At antenna B, the phase is offset because the distance between the antennas causes the propagation delay; therefore, the phase at antenna B is received in radians.

$$\varphi_B(t) = \varphi_A(o) + 2\pi f_o t \left(t - \frac{D(t)}{c}\right) \tag{2}$$

At antenna A $\varphi_A(o)$ is the initial phase, D(t) is the distance between the two antennas, and c is the velocity of light in a vacuum. The phase of the signal received by antenna B.

$$D(t) = R - (\overrightarrow{x_o}.\hat{r}\ ) sin\,(2\pi f_v t) \tag{3}$$

Substituting (3) into (2) and choosing the initial phase.

$$\varphi_B(t) = 2\pi f_o t \left(t + \frac{\overrightarrow{x_o}.\hat{r}}{c} sin\,(2\pi f_v t)\right) \tag{4}$$

Compute the second derivative of place (1) for time to get the peak acceleration.

$$\overrightarrow{a_p} = (2\pi f_v t)^2\ \overrightarrow{x_o} \tag{5}$$

There are 2 acceleration peaks of the same amplitude but in opposing directions. The max acceleration in the specified direction is provided for convenience of $\overrightarrow{x_o}$ was chosen for the definition of $\overrightarrow{a_p}$ .Solve (5) for $\overrightarrow{x_o}$ and substitute the result back into (4). The phase noise received by antenna B.

$$\varphi_B(t) = 2\pi f_o t + \frac{1}{2\pi}\frac{\overrightarrow{a_p}.\hat{R}}{c}\frac{f_o}{f_v^2} sin\ sin\,(2\pi f_v t) \tag{6}$$

f_o is the sin wave frequency, f_v is the vibrating frequency, $\overrightarrow{a_p}$is the peak acceleration, $\hat{R}$ the location of antenna B, c the speed of light. Fig. 3 depicts the main source of drone vibration [32]. The vibration of the drone is always random [33]. Modelling and collecting random vibrations in unmanned aerial vehicles or UAV systems is challenging since it is difficult to identify the different sources [34]. Undesired vibrations commonly originate from the primary rotor, engine, and

rechargeable battery energy source [35]. Sensitive electronic components in UAV systems can generate random vibrations with high random features due to responses to pavement roughness, acoustic pressure, and air disturbance [36]. This vital category of issues can lead the system to move from a stable state to a state of failure [37].

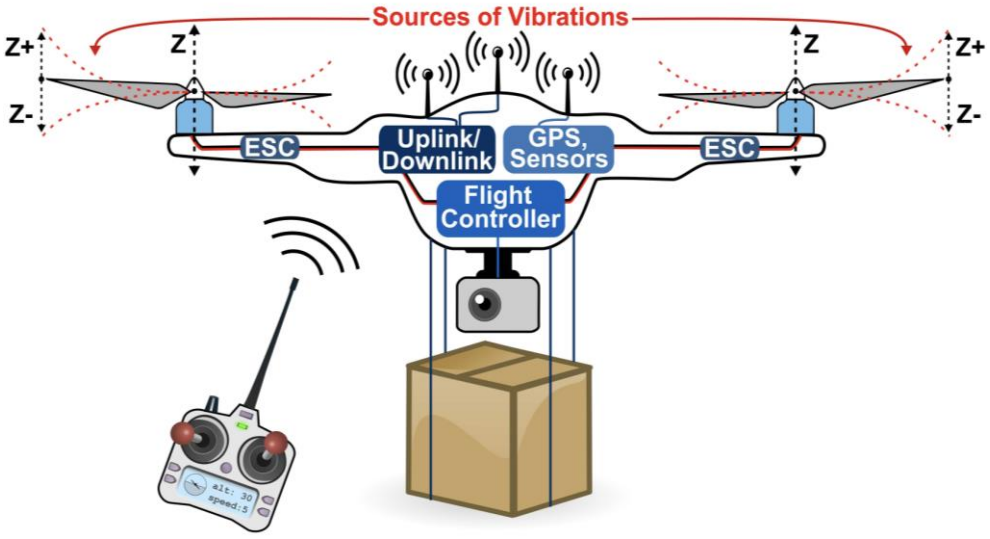

Fig. 3. Drone vibration sources

Random vibrations are typically characterized by their (PSD). Call the vibrational PSD in the direction $\hat{r}$ $G(\hat{r}.f_v)$ in unite of g²/Hz, where g is the acceleration of Earth's gravity. For a narrow bandwidth Δf_v of random vibration, the vibration is approximately sinusoidal and the peak acceleration can be related to the vibrational PSD [20].

$$a_p = g\sqrt{2\Delta f_v G(\hat{r}.f_v)} \tag{7}$$

The factor of (√2) scales from the RMS [38]. Write the phase received by antenna B as a function of the vibrational power spectral density (PSD) using the given equation and $\emptyset_o$ as the initial random phase of the vibration at t = 0. Where is the phase noise detected by antenna B due to random vibration [20].

$$\varphi_B(t) = 2\pi f_o t + \frac{1}{2\pi}\frac{g}{c}\frac{f_o}{f_v^2}\sqrt{2\Delta f_v G(\hat{r}.f_v)}\ sin\ sin\ (2\pi f_v t + \emptyset_o) \tag{8}$$

Where g Earth's gravity, $G(\hat{r}.f_v)$ the direction of acceleration of earth gravity=0.98 m/s2. Phase noise resulting from vibration affected the symbol error rate SER. Moreover, the probability density function PSD could be calculated for varying mapping orders(M-QAM) using Equations (8) and (9). [39]. The following is the PSD equation for the received signal under random vibration derived by [39].

$$f_{r_i x_i}(x,y) = N_2\left(a_{il}\sqrt{\frac{E_g}{2}}, a_{iQ}\sqrt{\frac{E_g}{2}}, \frac{a_{iQ}^2 E_g \theta_{rms}^2 + N_o}{2}, \frac{a_{il}^2 E_g \theta_{rms}^2 + N_o}{2}\right) \tag{9}$$

Where a_{il} and a_{iQ} are the two orthogonal components of the signal; $E_g$energy of the signal; θ phase noise for varying mapping orders, SER could be calculated using equation (4) derived by [39]. Where M is the order of mapping.

$$P_{e-MQAM} = \frac{1}{M}[1 - \sum_{i=1}^{M} \int_{ci}^{di} \int_{ai}^{bi} f_{\frac{r_i}{s_i}}(x,y)dxdy] \quad (10)$$

3. Theoretical Background

This section briefly discusses the phase noise effect communication system and the Convolution Neural Network (CNN) layers.

3.1. Phase Noise Effect Communication System

Drone vibration during flight produces phase noise. The Institute for Telecommunication Sciences defines phase noise (PN) as rapid, short-term, random variations in the phase of a wave in an oscillator resulting from time-domain instabilities. Phase Noise (PN) is a critical element in communication systems as it impacts the single receiver, affecting the symbol error rate (SER). Drone communication systems are moving towards higher QAM (quadrature amplitude modulation) schemes like 1024, 2048, or even 4096QAM to take advantage of increased capacity and throughput. In addition to trade-off considerations such as increased interference, reduced signal density, and signal coordination complexities, it is essential to factor in PN compared to AWGN as an additional trade-off element. This can further complicate the system's design, leading to additional costs.

In Fig. 4 we take 16-QAM and 64-QAM to compare the affected phase noise, the constellation diagram, and arrange symbols.

1. 16-QAM

a. Each symbol represents 4 bits (2 bits for amplitude and 2 bits for phase).

b. The constellation diagram contains a 4x4 grid (distinct point).

c. The constellation diagram symbols (phase angle 45 degrees).

d. The distance between the symbols is relatively large, making it less sensitive to phase noise compared to high-order QAM.

2. 64-QAM

a. Each symbol represents 6 bits (3 bits for amplitude and 3 bits for phase).

b. The constellation diagram contains an 8x8 grid (distinct point).

c. The constellation diagram symbols (phase angle 22.5 degrees).

d. The distance between the symbols is very close and therefore highly sensitive to phase noise compared with lower-order QAM.

So, high-order QAM provides a high data rate in the communication system when increasing the symbol's number and density in the constellation diagram. However, the high-density symbols lead to high sensitivity to noise and bit errors. Phase noise results in the rotation of points on a constellation diagram around the origin. High-order QAM, like 16-QAM, 64-QAM, or higher, requires placing symbols more densely in a complicated plane. Phase noise shifts constellation points from their ideal locations, leading to symbol errors. High-order QAM includes symbols that are close together, causing them to interfere with adjacent symbols and causing a higher bit error rate (BER). Phase noise can cause inter-symbol interference by allowing the phase noise of one symbol to impact adjacent symbols. Interference disrupts the signal and may interfere with the receiver's ability to accurately demodulate symbols, especially with high-order QAM with closely spaced symbols.

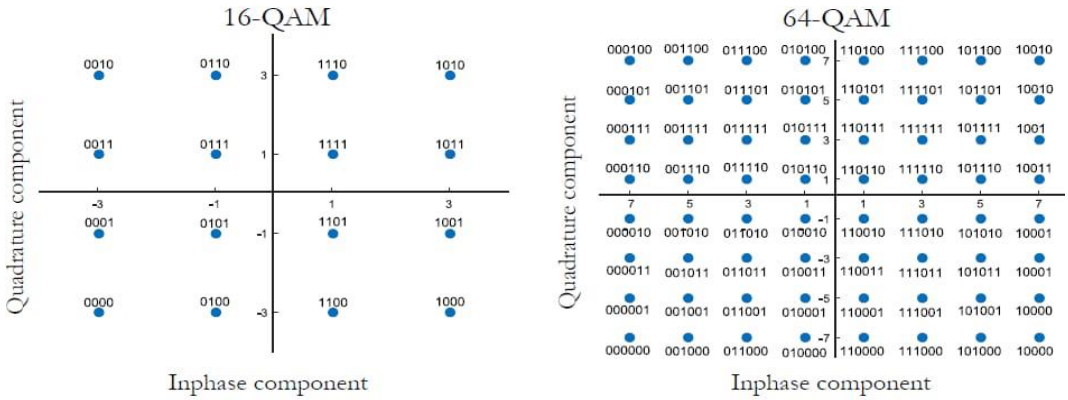

Fig. 4. Constellation diagram for 16-QAM vs 64-QAM

Phase noise often increases with higher offset frequencies from the carrier frequency. In simple terms, the phase noise power spectral density increases at higher frequencies further from the carrier. So, the high-frequency elements of the QAM signal that are far from the carrier frequency face more phase noise, causing increased distortion. In short. Phase noise impacts all frequency components of a signal. However, it significantly impacts high-frequency components in high-order QAM systems because of their wider bandwidth, more excellent symbol rates, and the spectrum features of phase noise.

3.2. Convolution Neural Network (CNN)

CNN operates based on the same principle as the natural visual system. CNN's distinctive architecture helps reduce overfitting in the neural network and decreases the computing cost of classification. The CNN design consists of layers: an output, an input, a fully connected (FCL), a pooling (PL), and a convolutional (CL)., as shown in Fig. 5 [40].

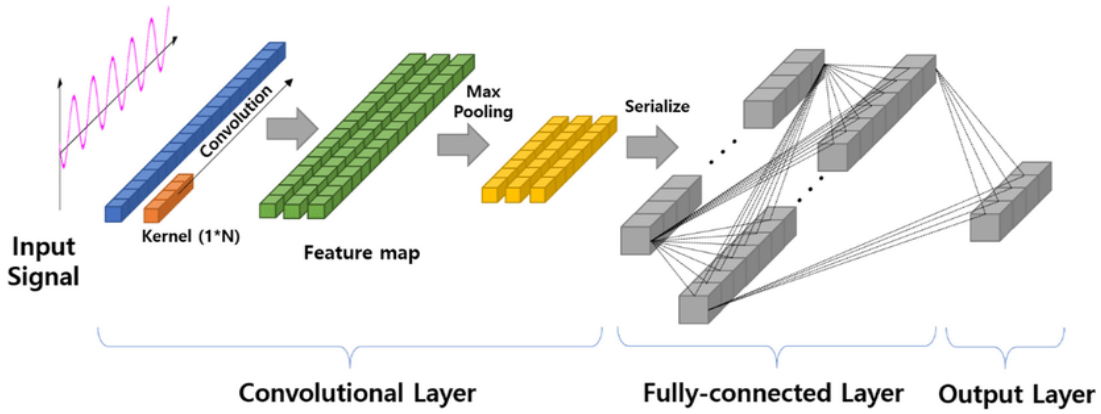

Fig. 5. CNN with four layer

The convolutional layer in a CNN extracts complex and abstract features from the input data. Using an activation function with varied weights and biases can increase the abstract features of the convolutional layer. The convolutional process of CNN is depicted in an equation (10).

$$x_l^j = f\left(\sum_{i \in Pn} x_i^{j-1} * w_{il}^j + b_l^j\right) \tag{11}$$

Where l: no. of layers; j component; w: weight; b: basis. Adding a pooling layer into the CNN enhances the quality of features obtained from the convolutional layer, as discriminant features have an essential role in accurate classification by a classifier.

$$x_l^j = f\left(w_l^j * \max\left(x_i^{j-1}\right) + b_l^j\right) \quad (12)$$

Where x_l^j: the max pooling operation. CNN utilizes numerous of layers of convolution and pooling to enhance its ability to extract local information from the input data. The CNN classifies data into appropriate categories after extracting hidden data using the pooling and convolutional layers. CNN utilizes a fully connected layer for this purpose. Equation (12) represents a fully connected layer that classifies the latent characteristics obtained using the convolution kernel [41].

$$fx^{j+1} = \left(\sum_{i=1}^{n} w_{il}^j a^{j(i)} + b_l^j\right) \quad (13)$$

The conventional deep CNNs presented in the previous section are designed to operate exclusively on 2D data, such as images and videos. This is why they are often referred to as ‘‘2D CNNs.” As an alternative, a modified version of 2D CNNs called 1D Convolutional Neural Networks (1D CNNs) has recently been developed [42]-[51]. These studies have shown that for certain applications, 1D CNNs are advantageous and thus preferable to their 2D counterparts in dealing with 1D signals due to the following reasons: There is a notable contrast in computational complexity between 1D and 2D convolutions. Specifically, convolving an image with N*N dimensions using a K*K kernel results in a computational complexity of approximately O~(N^2K^2) for 2D convolution and approximately O~(NK) for 1D convolution with the same dimensions. Under identical conditions, the computational complexity of a 1D CNN is notably lower than that of a 2D CNN. And recent studies show that 1D CNN applications typically use compact configurations with 1-2 hidden CNN layers and networks with less than 10,000 parameters. In contrast, 2D CNN applications commonly use deep architectures with over 1 million parameters, often exceeding 10 million. Shallow networks are easier to train and implement compared to deep networks. And training deep 2D CNNs typically necessitates specialized hardware configurations, such as cloud computing or GPU farms. CPU implementation on a regular computer is possible and quite quick for training small 1D CNNs with few hidden layers (e.g., 2 or less) and neurons (e.g., less than 50).

In this study, we utilized a one-dimensional convolutional neural network (CNN) to detect vibration effects. CNN is utilized as a component for extracting characteristics. We implemented 1DCNN using the dataset provided by the simulation. The following approach was used: (a) A new dataset was created by dividing the original dataset into a training set and a validation set; (b) The dataset was trained using 1DCNN in MATLAB for regression; (c) Following training, performance metrics such as Mean Squared Error, Root Mean Absolute Error, Mean Absolute Error, and Relative Error were calculated; (e) Subsequently, the code was converted into a user-friendly platform using App MATLAB Designer, improving accessibility and usability.

4. Methodology

To predict the symbol error rate (SER) causing the effect of phase noise from the vibration on the drone's communication system, we will use the following two methods:

4.1. Theoretical Model of Monte Carlo Simulation

Monte Carlo simulations are essential to evaluating the impact of vibration on drone communication systems due to their ability to model complex systems with different parameters while running multiple simulation trials with random variations, providing information regarding system performance. Monte Carlo simulations provide accurate estimations of system performance based on average findings from multiple simulation attempts, which is crucial for evaluating the effects of phase noise [52].

The impact of drone vibration on communication systems, specifically the 5.8 GHz and 2.4 GHz frequencies that drones use to send data and video, almost all drones use them and their free licenses. The vibration frequency ranged from 10 to 100 Hz [53], and the other variables' values are in Table 1.

Table 1. The parameters used in the simulation

Parameters	Variables	
	Value	Description
Modulation order(M)	4Qam,16Qam,32Qam	Number of symbols in QAM modulation
Signal to Noise Ratio (SNR)	-2 to 10	ratio of signal power to noise power
Vibration Amplitude (A)	0. 1 to 2	amplitude of the antenna vibration
Carrier Frequency (f_c)	2.4GHz, 5.8 GHz	frequency of the carrier signal
Vibration Frequency (f_m)	10 Hz, 100Hz	frequency of the antenna vibration
Number of Iteration	100-500	number of iterations for the Monte Carlo simulation
Noise Standard Deviation (sigma)	0.1	standard deviation of the additive white Gaussian noise

The Monte Carlo approach is used in this section to determine the performance simulation, validate the estimated results, and gain a deeper understanding of the vibration's influence. It gives a clearer picture than a deterministic forecast [54]. The simulation was conducted using MATLAB 2021b, and the program flow chart is displayed in Fig. 6.

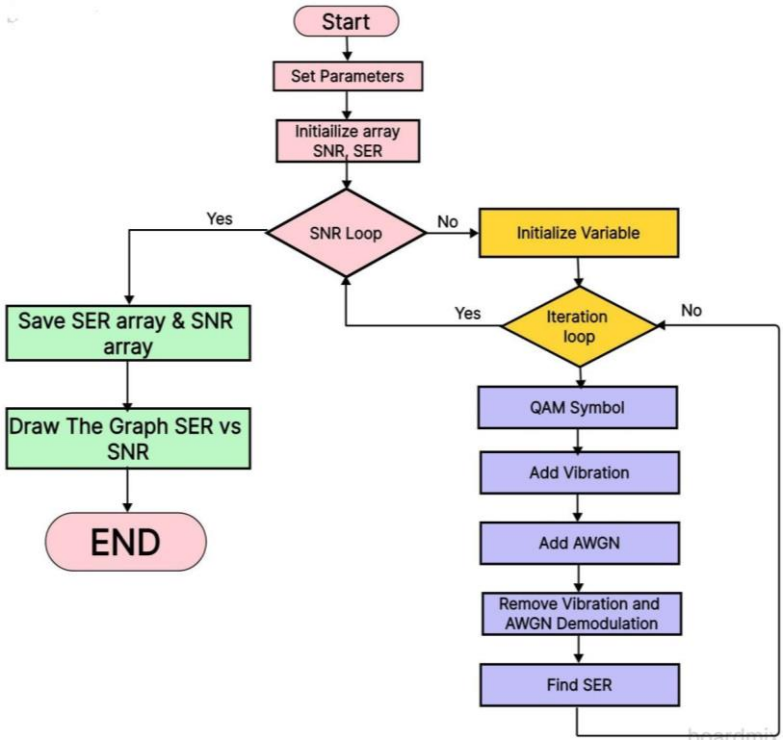

Fig. 6. Flow chart of simulation

Fig. 6 shows the steps of the algorithm to estimate the effect on the communication system on the drone. By following the steps:

1. Set the variable value in the theoretical simulation in MATLAB as shown in Fig. 7.
2. At the transmitter side, we randomly generate QAM symbols (x) to generate the signal and modulate these symbols.

3. Adding AWGN to the affected signal. Now that the signal has affected the noise affected.by vibration
4. At the receiver side, after receiving the signal, we will remove the vibration effect and demodulate.
5. Then count and compare the error symbols with the original symbols. To compute the SER. The expressions of the SER of the M-QAM system due to the vibrating antenna are shown based on the proposed model.
6. Repeat this procedure deepened on the iteration number set first. With a high number of iterations, SER will get high-accuracy results to SER.

```
M = 16;                  % Number M_QAM order
num_iter = 100;          % number of iterations
f_m = 10:10:100;         %  Define vibrational frequencies range
A = 3;                   % amplitude Vibration
SNR_dB_range = -2:2:10; % Define ranges SNR_dB
f_c = 2.4e9;             % Frequency Carrier
```

Fig. 7. Parameters of MATLAB simulation

Note: Change the parameters in the simulation to different values and take all cases as shown in Table. 1.

4.2. One-Dimension Convolution Neural Networks (1DCNN)

The traditional method uses the simulation theoretical model to estimate the effect of phase noise produced by drone vibrations. However, we will use deep learning (DL) to train and test our model on the data set we collected. After that, we can use it with a comprehensive data range. Deep learning is a branch of AI used in different fields [55], [56]. One of the most critical factors in CNN is the decreased number of parameters in artificial neural networks (ANN) [57]-[58]. CNN is a widely used DL architecture that can be trained directly from input data without requiring manual feature extraction [59]-[61].

4.2.1. CNN Architecture

Designed the modal CNN to be suitable for learning the relationship between parameter input and their SER cross-ponding.

1. Input layer: define the data input size in this layer. We have five columns and one row labeled.
2. Convolution layer: We use two layers with 16 filters of size 3x3 for the kernel to extract significant features. The kernel of the convolutional layer consists of values (weights) that are convolved with the input data to generate feature maps. Empirical research has demonstrated that networks utilizing 3x3 filters typically perform various tasks. The common use of 3x3 filters in successful structures confirms their efficacy. Choosing a 3x3 filter size in convolutional layers provides a balance between obtaining local features, parameter efficiency, and getting optimal performance in various tasks. Padding the output dimensions to match the input dimensions.
3. Relu layer: applies the activation function to the output of the convolution layer to make it non-linear.
4. Fully connected layer: We use two layers contains weights, biases, and neurons to establish connections between neurons in different layers. The layers are typically positioned before the output layer and constitute the last layers of a CNN architecture. • This layer has a single neuron that generates a value indicating the predicted SER.

5. Regression layer: calculates the error between the predicted and actual outputs. Primarily used for regression assignments, such as predicting continuous values like the symbol error rate (SER).

After the CNN architecture has been planned. To process the dataset, Follow steps flow chart of 1DCNN in Fig. 8.

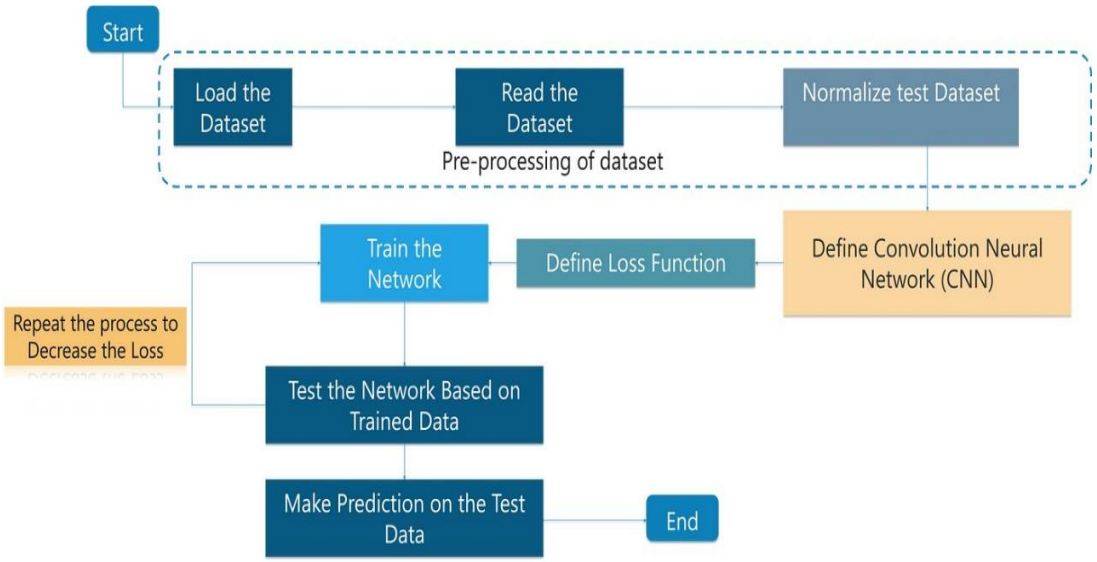

Fig. 8. Flow chart of CNN

4.2.2. Dataset Collection

Firstly, we generated the dataset from the previous simulation, as shown in Table 2. Containing five columns (M-QAM, carrier frequency, amplitude vibration, frequency vibration, and SNR), all these parameters have various levels. Label each set with the corresponding SER, which represents the one set for which we generate 8000 rows. During the data collection phase, we faced the challenge of insufficient data provided by simulation. We need to create more data sets to address this limitation and improve accuracy.

Table 2. The sample of dataset using in CNN

Dataset parameters				
M-QAM	**Amplitude-Vibration**	**Frequency-Carrier**	**SNR**	**Frequency -vibration**
4	0.1	2.4	-2	100
16	0.9	2.4	0	82
32	1	5.8	8	10
64	2	5.8	4	24

4.2.3. Regression

After loading the dataset as in Fig. 8. Into the input layer to reprocess the dataset, the next step is to split the data into 70% training and 30% testing to evaluate the modal performance and measure the accuracy. So to predict the SER value, utilize regression techniques, particularly 1DCNN (Convolutional Neural Network) regression. This advanced technology enables us to project continuous numerical values. We utilized CNN regression and computed multiple measures to evaluate the accuracy of our predictions. The metrics consist of Mean Square Error (MSE), Root Mean Square Error (RMSE), Mean Absolute Error (MAE), Root Mean Absolute Error (RMAE), and Relative Error (RAE), as shown in the equations:

1. Mean square error (MSE).

$$MSE = \frac{1}{n}\sum_{i=1}^{n}(y_i - \hat{y_i})^2 \quad (14)$$

2. Root mean square error (RMSE).

$$RMSE = \sqrt{MSE} \quad (15)$$

3. Mean Absolute Error (MAE).

$$MAE = \frac{1}{n}\sum_{i=1}^{n}|y_i - \hat{y_i}| \quad (16)$$

4. Root Mean Absolute Error (RMAE).

$$RMAE = \sqrt{MAE} \quad (17)$$

5. Relative Error (RAE).

$$RAE = \frac{1}{n}\sum_{i=1}^{n}\left|\frac{y_i - \hat{y_i}}{y_i}\right| \times 100\% \quad (18)$$

Where n : no. of samples; y_i: actual value; $\hat{y_i}$ predicated value. By calculating these metrics, we can comprehensively evaluate the performance of our CNN regression model in predicting the vibration effect to symbol error rate SER. This allows us to evaluate accuracy and improve the regression rraining process.

4.2.4. MATLAB App Designer

The regression training was completed, and the system evaluation parameters were calculated. The code was transformed into a platform that is easy to use via MATLAB App Designer, which is an intelligent method to enhance accessibility and usability. App Designer enables the development of interactive MATLAB apps through an easy-to-use graphical user interface (GUI). The design was finalized, as depicted in Fig. 9.

Fig. 9. Predicts the effect of vibration on symbol error rate (GUI)

The first field has a drop-down list representing the M-QAM order (4-QAM, 16-QAM, 32-QAM,64-QAM), while the second field has a drop-down list representing the type frequency carrier (2.4 GHz, 5.8 GHz). Moreover, the third field represents the amplitude vibration, the fourth field represents the frequency vibration, and the last field represents the signal-to-noise ratio SNR. When the check button is pressed, the SER value appears in the SER field, as shown in Fig. 9.

In short, we generated the dataset from the previous simulation, which contained five columns (M-QAM, frequency vibration, frequency amplitude, frequency carrier, and SNR), all parameters with various levels. Label each set with the corresponding SER and process the data by normalizing the input data and encoding the labels to be compatible with the data format to train the CNN. Designed the modal CNN to be suitable for learning the relationship between parameter input and their SER cross-ponding. After that, the dataset goes to the input layer, the last split of the data goes to 70% training and 30% testing to evaluate the modal performance and measure the accuracy of extracting the feature from the input in the convolution layer, reducing the dimension in the pooling layer, combining the feature data, and predicting the effect in the fully connected layer; the output is the SER predicted in the output layer; and the last step is created (GUI) by MATLAB App Designer.

5. The Results

5.1. Theoretical Model of Monte Carlo Simulation

In the same way, as described above in Mote Carlo's method chapter, the simulation is carried out with MatLab 2021b by employing the algorithm as a Monte Carlo iteration simulation with several variable values. This is done to observe the impact of vibration on the various statuses and to measure the symbol error rate (SER).Initially, we used a carrier frequency of 2.4 GHz and a vibration frequency of 10 Hz and 100 Hz to draw SERs with various SNRs and orders (4QAM, 16QAM, and 32QAM). The second experiment used a carrier frequency of 5.8 GHz, vibration frequencies of 10 and 100 Hz, and orders 4QAM, 16QAM, and 32QAM. The number of iterations was equal to 100, as shown in Fig. 10.

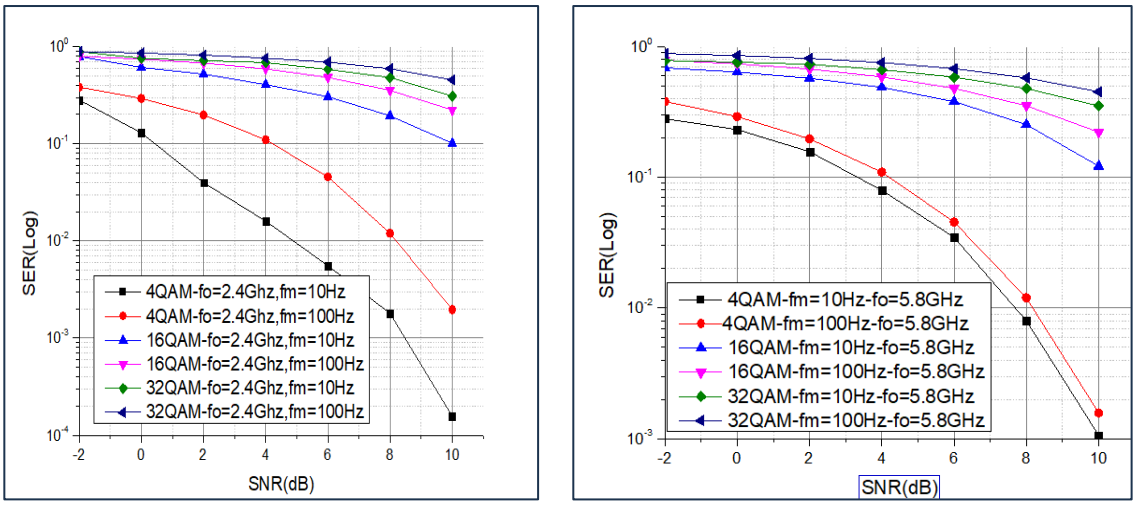

Fig. 10. SER vs. SNR for different order of QAM and carrier frequency

As shown in Fig. 10, phase noise generated by drone vibrations leads to the symbol error rate SER increasing when the QAM order and frequency of the vibration increase because the symbols are closer to each other as 64-QAM is more sensitive than others.

Fig. 10. shows the relationship between signal-to-noise ratio SNR and symbol error rate SER and represents them as curves. At high SNR levels, the SER decreases because the signal strength is

higher than the noise level. So, it is easy to distinguish between the different symbols. At a low SNR level, the SER increases because the signal strength is lower than the noise level. So it is difficult to recover between the different symbols.

Fig. 11. shows the relationship between the SER and the number of iterations for both of the carrier frequencies, which are 2.4 GHz and 5.8 GHz. The carrier frequency and vibration frequency have a more significant influence on the signal that is received. It is clear from the information presented above that random antenna vibration affects the communications system of the drone. This is especially true when the carrier frequency and vibration frequency are increased and when a higher M-QAM order is chosen.

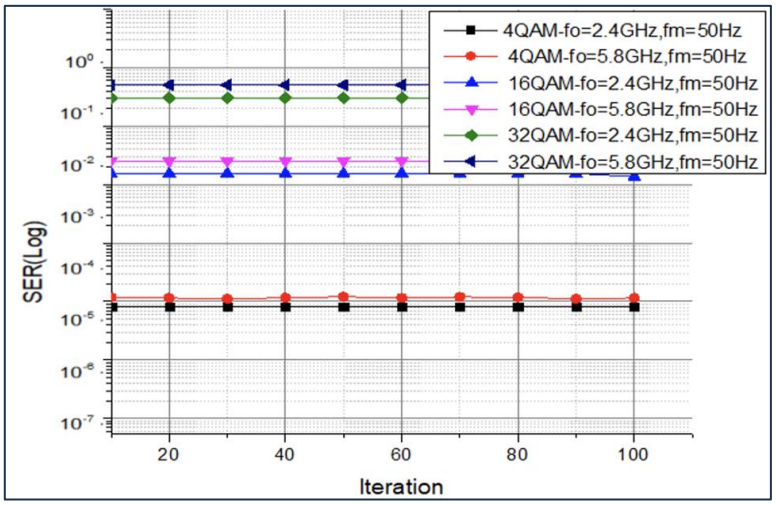

Fig. 11. SER vs iteration for different MQAM

So, we notice from the result that the high value symbol error rate SER (0.6738247) comes from a high carrier frequency of 5.8 GHz, a high vibration frequency of 100 Hz, and a high M-QAM order of 64-QAM. We notice how degrading the drone communication system's performance is when we increase the carrier frequency and use high-order M-QAM. This is conducted to assess the influence of vibration on different conditions and to quantify the symbol error rate (SER).

5.2. One-Dimension Convolution Neural Networks (1DCNN)

After making the architecture model, collecting and loading the dataset, and then making the training and regression stages, as shown in Fig. 12, the regression training process is performed in 1DCNN.

The result of training and testing appears to be good accuracy in Fig. 13. Which appear the validation rout mean square error (RMSE) is 2.89772, and by calculating some metrics, as shown in the method chapter, we can comprehensively evaluate the performance of the CNN regression model in predicting the vibration effect on the communication system by measuring the symbol error rate (SER). This allows us to evaluate performance and improve as needed. Enhance training results by ensuring dataset equality and diversity, and by increasing dataset size.

In Fig. 13. show the visualized predictions. The x-axis represents the true values, and the y-axis represents the predicted values. We notice the regression line crossing above the diagonal line (representing the perfect prediction). In Fig. 14. show the visualized predicted value matches the true value, which means a high evaluation performance from our CNN model.

After fine-tuning parameters such as epochs, batch size, and learning rate, etc., to achieve optimal performance, The system's overall performance was assessed, and the parameters for the evaluation were calculated as shown in Table 3.

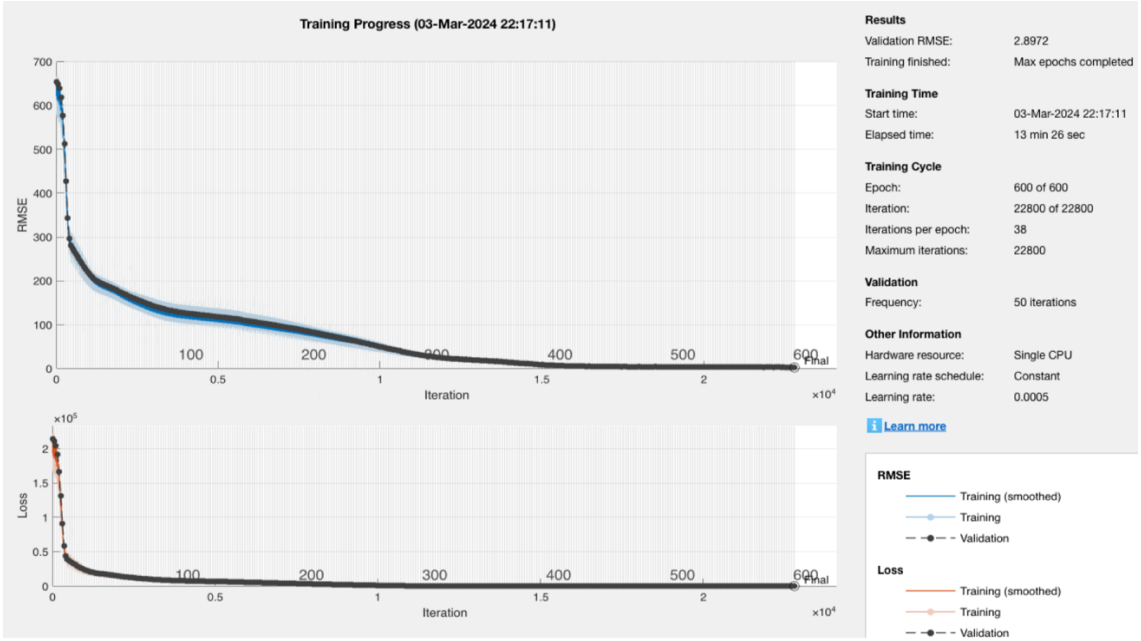

Fig. 12. Regression Training process

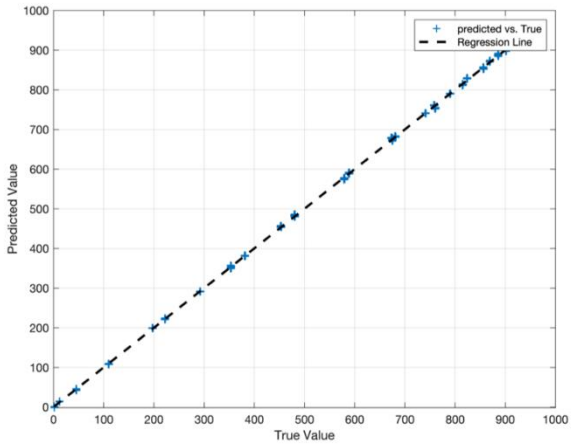

Fig. 13. Visualize prediction values vs. true values

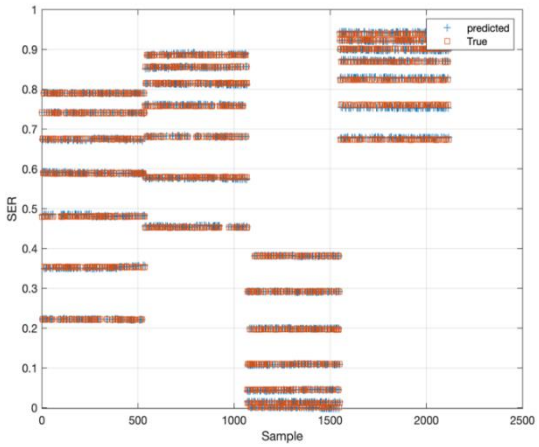

Fig. 14. Visualize sample values vs. ser values

Table 3. Evolution parameters of regression

Parameters	Value
Mean square error (MSE)	8.392
Root mean square error (RMSE)	2.897
Mean Absolute Error (MAE)	2.301
Root Mean Absolute Error (RMAE)	1.516
Relative Error (RAE)	0.000116 %

The CNN method results after processing input data through numerous layers, learning representations at each stage, and producing a prediction of the SER as the output. Training uses kernel parameters to extract essential characteristics from the input data. We notice that the symbol error rate (SER) also increases when the vibration and carrier frequencies, as well as the order QAM,

increase. Because of the phase noise produced by the vibration effect on bits in the constellation QAM.

Table 4. Sample of Results

Parameters input					Result
M-QAM	**Freq-Carrier**	**Freq-Vibration**	**Amp-Vibration**	**SNR**	**SER**
64	2.4	100	2	10	0.6738749
32	2.4	100	2	10	0.4533443
16	2.4	100	2	10	0.2220764
4	2.4	100	2	10	0.1562560
64	5.8	100	2	10	0.6738247
32	5.8	100	2	10	0.4530797
16	5.8	100	2	10	0.2220262
4	5.8	100	2	10	0.1567030

Table. 4 shows the results obtained using TL1DCNN. It indicates that increasing the number of frequency carriers, vibration frequency, and modulation order in M-QAM leads to a deterioration in the drone communication system's performance. The vibrating antenna is responsible for these effects. Our contribution lies in employing TL1DCNN, while other studies rely solely on simulation to assess drone communication system performance. This study offers a valuable method to evaluate the efficiency of a communication system on a drone. 1DCNN can automatically extract useful features from the input dataset to evaluate the effect, which is particularly important for wireless system drone planning.

6. Discussion

Most of the previous research focused on using simulations or experiments to show the effect of the vibration drone on communication systems, as mentioned in the introduction section. In this paper, we use the one-dimensional neural network (1D CNN) to examine the effect of vibration on the communication system of a drone by measuring the symbol error rate (SER). We then create the dataset by using the theoretical simulation as the algorithm mentioned in the method section, process the data set, upload it to our CNN model, and tune parameters (epoch, number iteration, bitch size, etc.) to get the best performance possible for the CNN model. The result appears to be a high vibration effect when using high-frequency carreri and high-order (M-QAM) with high vibration frequency.

Using 1DCNN to analyze the effect of drone vibrations on communication systems has some limitations, such asFor training 1DCNN, the dataset contains vibrations and performance communication system data, which is difficult to collect with high equality and diversity. The real-world environment presents a unique challenge for UAVs, like varying conditions and unpredictable vibrations. The model's training is hindered in adapting to this challenge. This study provides a valuable method to evaluate the efficiency of a communication system on the UAV, which is particularly important for drone wireless system planning. In the following work, we propose implementing a feedback loop between the CNN result and communication system to adjust the system parameters to improve performance, such as modulation order and power transmission, and investigating other factors affecting UAV communication systems, including humidity and temperature.

7. Conclusion

In this work, we study drone vibrations that produce phase noise and how phase noise affects the drone communication system, which can negatively impact the operation of wireless communication systems, using two methods. The first stage uses the simulation Monte Carlo in MatLab 2021b when the iteration algorithm processes with various variable values as the frequency

carriers (2.4 GHz, 5.8 GHz) and the order of the M-QAM system (4-QAM, 16-QAM, 32-QAM, or 64-QAM) and evaluates the performance of the communication system on the drone by measuring the symbol error rate SER. The second stage uses the convolutional neural network CNN to predict the symbol error rate (SER). After training and testing our model in the dataset that is created in simulation, the MATLAB App Designer creates a GUI that is easy and friendly for the user.

So, we notice from the result that the high value symbol error rate SER (0.6738247) comes from a high carrier frequency of 5.8 GHz, a high vibration frequency of 100 Hz, and a high M-QAM order of 64-QAM. We notice how degrading the drone communication system's performance is when we increase the carrier frequency and use high-order M-QAM. This is conducted to assess the influence of vibration on different conditions and to quantify the symbol error rate (SER).

Theoretical reason that High-order QAM provides a high data rate in the communication system when increasing the symbol's number and density in the constellation diagram. However, the high-density symbols lead to high sensitivity to noise and bit errors. Phase noise results in the rotation of points on a constellation diagram around the origin. High-order QAM, like 16-QAM, 64-QAM, or higher, requires placing symbols more densely in a complicated plane. Phase noise shifts constellation points from their ideal locations, leading to symbol errors. High-order QAM includes symbols that are close together, causing them to interfere with adjacent symbols and causing a higher bit error rate (BER). Phase noise can cause inter-symbol interference by allowing the phase noise of one symbol to impact adjacent symbols. Interference disrupts the signal and may interfere with the receiver's ability to accurately demodulate symbols, especially with high-order QAM with closely spaced symbols.

Phase noise often increases with higher offset frequencies from the carrier frequency. In simple terms, the phase noise power spectral density increases at higher frequencies further from the carrier. So, the high-frequency elements of the QAM signal that are far from the carrier frequency face more phase noise, causing increased distortion.

To reduce the impact of vibrations on the drone communication system, implement some methods, such as mechanical isolation between the frame and communication components on the drone, digital signal processing technology to filter noise from signals received, and other methods to optimize flight control algorithms (PID, proportional integer derivative).

Using 1DCNN to analyze the effect of drone vibrations on communication systems has some limitations, such as. The dataset contains vibrations and performance communication system data for training 1DCNN, which is difficult to collect with high equality and diversity. The real-world environment presents a unique challenge for UAVs, like varying conditions and unpredictable vibrations. make the model trained suffer in its ability to adapt to this challenge.

Our contribution to this work is using 1DCNN, unlike other works that only use simulation to evaluate the performance of the UAV communication system. This study provides a valuable method to evaluate the efficiency of a communication system on the UAV, which is particularly important for drone wireless system planning. In the following work, we propose implementing a feedback loop between the CNN result and communication system to adjust the system parameters to improve performance, such as modulation order, power transmission, and investigating other factors affecting UAV communication systems, including humidity and temperature.

Author Contribution: All authors equally contributed to this paper's significant contribution. All authors reviewed and approved the work.

Funding: This research was self-funded.

Conflicts of Interest: No authors declare conflicts of interest.

References

[1] K. Telli, O. Kraa, Y. Himeur, A. Ouamane, M. Boumehraz, S. Atalla, and W. Mansoor, "A comprehensive review of recent research trends on unmanned aerial vehicles (uavs)," *Systems*, vol. 11, no. 8, p. 400, 2023, https://doi.org/10.3390/systems11080400.

[2] P. -H. Chu, Y. T. Huang, C.-H. Pi, and S. Cheng, "Autonomous Landing System of a VTOL UAV on an Upward Docking Station Using Visual Servoing," *IFAC-PapersOnLine*, vol. 55, no. 27, pp. 108-113, 2022, https://doi.org/10.1016/j.ifacol.2022.10.496.

[3] N. Sethi and S. Ahlawat, "Low-fidelity design optimization and development of a VTOL swarm UAV with an open-source framework," *Array*, vol. 14, p. 100183, 2022, https://doi.org/10.1016/j.array.2022.100183.

[4] T. Patel, M. Kumar, and S. Abdallah, "Control of Hybrid Transitioning Morphing-wing VTOL UAV," *IFAC-PapersOnLine*, vol. 55, no. 37, pp. 554-559, 2022, https://doi.org/10.1016/j.ifacol.2022.11.241.

[5] M. Bahari, M. Rostami, A. Entezari, S. Ghahremani, and M. Etminan, "A comparative analysis and optimization of two supersonic hybrid SOFC and turbine-less jet engine propulsion system for UAV," *Fuel*, vol. 319, p. 123796, 2022, https://doi.org/10.1016/j.fuel.2022.123796.

[6] M. Bahari, M. Rostami, A. Entezari, S. Ghahremani, and M. Etminan, "Performance evaluation and multi-objective optimization of a novel UAV propulsion system based on PEM fuel cell," *Fuel*, vol. 311, p. 122554, 2022, https://doi.org/10.1016/j.fuel.2021.122554.

[7] K. Zhou *et al*., "A kW-level integrated propulsion system for UAV powered by PEMFC with inclined cathode flow structure design," *Applied Energy*, vol. 328, p. 120222, 2022, https://doi.org/10.1016/j.apenergy.2022.120222.

[8] M.-A. Stamate, C. Pupăză, F.-A. Nicolescu, and C.-E. Moldoveanu, "Improvement of Hexacopter UAVs Attitude Parameters Employing Control and Decision Support Systems," *Sensors*, vol. 23, no. 3, p. 1446, 2023, https://doi.org/10.3390/s23031446.

[9] N. Li, X. Liu, B. Yu, L. Li, J. Xu, and Q. Tan, "Study on the environmental adaptability of lithium-ion battery powered UAV under extreme temperature conditions," *Energy*, vol. 219, p. 119481, 2021, https://doi.org/10.1016/j.energy.2020.119481.

[10] B. Turetken and M. Celik, "Analysis of vibration effects on surface matched cylindrical IFF array antenna," *2013 7th European Conference on Antennas and Propagation (EuCAP)*, pp. 2731-2735, 2013, https://ieeexplore.ieee.org/abstract/document/6546794.

[11] N. Jekabsons and S. Upnere, "Coupled structural-electromagnetic numerical modeling and analysis of large reflector antenna," *2015 IEEE-APS Topical Conference on Antennas and Propagation in Wireless Communications (APWC)*, pp. 708-711, 2015, https://doi.org/10.1109/APWC.2015.7300177.

[12] P. Xu *et al*., "Structural-Electromagnetic-Thermal Coupling Technology for Active Phased Array Antenna," *International Journal of Antennas and Propagation*, vol. 2023, 2023, https://doi.org/10.1155/2023/2843443.

[13] W. Cong-si, K. Ming-kui, W. Wei, P. Tao, "Analysis of electrical performances of phased array antennas with structural deformations," *Journal of Systems Engineering and Electronics*, vol. 35, no. 8, pp. 1644-1649, 2013, https://doi.org/10.3969/j.issn.1001-506X.2013.08.10.

[14] C. D. Rodin, F. A. D. A. Andrade, A. R. Hovenburg, and T. A. Johansen, "A survey of practical design considerations of optical imaging stabilization systems for small unmanned aerial systems," *Sensors*, vol. 19, no. 21, p. 4800, 2019, https://doi.org/10.3390/s19214800.

[15] A. Madhag and H. Z. Dhaam, "Satellite vibration effects on communication quality of OISN system," *Open Engineering*, vol. 12, no. 1, pp. 1113-1125, 2022, https://doi.org/10.1515/eng-2022-0355.

[16] O. Bektash and A. L. Cour-Harbo, "Vibration analysis for anomaly detection in unmanned aircraft," *Annual Conference of the Prognostics and Health Management Society*, vol. 12, no. 1, p. 10, 2020, https://doi.org/10.36001/phmconf.2020.v12i1.1143.

[17] M. Arif and W. Kim, "Analysis of Fluctuating Antenna Beamwidth in UAV-Assisted Cellular Networks," *Mathematics*, vol. 11, no. 22, p. 4706, 2023, https://doi.org/10.3390/math11224706.

[18] H. -A. Hou and L. -C. Wang, "Analysis on Time-Variant Air-to-Ground Radio Communication Channel for Rotary-Wing UAVs," *2019 IEEE 89th Vehicular Technology Conference (VTC2019-Spring)*, pp. 1-6, 2019, https://doi.org/10.1109/VTCSpring.2019.8746377.

[19] M. Banagar, H. S. Dhillon and A. F. Molisch, "Impact of UAV Wobbling on the Air-to-Ground Wireless Channel," *IEEE Transactions on Vehicular Technology*, vol. 69, no. 11, pp. 14025-14030, 2020, https://doi.org/10.1109/TVT.2020.3026975.

[20] W. Cong-si, K. Ming-kui, W. Wei, "On coupled structural-electromagnetic model of active phased array antennas with array plane structural distortion errors," *Acta Electronica Sinica*, vol. 42, no. 12, pp. 2520-2526, 2014, https://doi.org/10.3969/j.issn.0372-2112.2014.12.027.

[21] L. Fan, L. L. Lv, F. J. Peng, G. P. Cai, "Coupled structural-electromagnetic modeling and analysis of active membrane phased array antenna," *Advances in Space Research*, vol. 66, no. 4, pp. 760-770, 2020, https://doi.org/10.1016/j.asr.2020.04.049.

[22] T. Takahashi *et al*., "On-Board Calibration Methods for Mechanical Distortions of Satellite Phased Array Antennas," *IEEE Transactions on Antennas and Propagation*, vol. 60, no. 3, pp. 1362-1372, 2012, https://doi.org/10.1109/TAP.2011.2180303.

[23] A. V. Nerobeev, A. N. Yakimov, A. R. Bestugin and I. A. Kirshina, "Radiation investigation of the antenna array, taking into account vibration actions," *2018 Systems of Signals Generating and Processing in the Field of on Board Communications*, pp. 1-4, 2018, https://doi.org/10.1109/SOSG.2018.8350624.

[24] H. Schippers and G. Vos, "On DOA estimation of vibrating antenna arrays," *2010 IEEE International Symposium on Phased Array Systems and Technology*, pp. 1010-1016, 2010, https://doi.org/10.1109/ARRAY.2010.5613235.

[25] T. Zhang, Z. Lv, W. Yin, M. Ke, G. Li, and Z. Ding, "Effect analysis of antenna translation vibration on GEO SARimage," *The Journal of Engineering*, vol. 2019, no. 20, pp. 6421-6425, 2019, https://doi.org/10.1049/joe.2019.0449.

[26] J. S. Ward, "Phase Noise Induced by a Vibrating Antenna," *IEEE Transactions on Microwave Theory and Techniques*, vol. 65, no. 11, pp. 4148-4153, 2017, https://doi.org/10.1109/TMTT.2017.2699682.

[27] I. M. Kilgore, S. A. Kabiri, A. W. Kane and M. B. Steer, "The Effect of Chaotic Vibrations on Antenna Characteristics," *IEEE Antennas and Wireless Propagation Letters*, vol. 15, pp. 1242-1244, 2016, https://doi.org/10.1109/LAWP.2015.2503264.

[28] A. Ranjan, P. Misra and H. B. Sahu, "Experimental measurements and channel modeling for wireless communication networks in underground mine environments," *2017 11th European Conference on Antennas and Propagation (EUCAP)*, pp. 1345-1349, 2017, https://doi.org/10.23919/EuCAP.2017.7928854.

[29] A. Kumar, S. Prince, N. Vedachalam and V. D. Prakash, "Ocean water channel modeling and estimation of power link budget for underwater wireless link," *2017 International Conference on Wireless Communications, Signal Processing and Networking (WiSPNET)*, pp. 1369-1372, 2017, https://doi.org/10.1109/WiSPNET.2017.8299987.

[30] B. Holfeld *et al*., "Radio channel characterization at 5.85 GHz for wireless M2M communication of industrial robots," *2016 IEEE Wireless Communications and Networking Conference*, pp. 1-7, 2016, https://doi.org/10.1109/WCNC.2016.7564890.

[31] H. Mingchao, Z. Pengbo, L. Haoyan, S. Guoliang and J. Shuqiang, "Performance Analysis of Wireless Communication System Affected by Vibrating Antenna," *2020 IEEE 20th International Conference on Communication Technology (ICCT)*, pp. 858-862, 2020, https://doi.org/10.1109/ICCT50939.2020.9295692.

[32] P. Nguyen *et al*., "DroneScale: drone load estimation via remote passive RF sensing," *Proceedings of the 18th Conference on Embedded Networked Sensor Systems*, pp. 326–339, 2020, https://doi.org/10.1145/3384419.3430778.

[33] M. Abdulrahman Al-Mashhadani, "Random vibrations in unmanned aerial vehicles, mathematical analysis and control methodology based on expectation and probability," *Journal of Low Frequency Noise, Vibration and Active Control*, vol. 38, no. 1, pp. 143–153, 2019, https://doi.org/10.1177/1461348418813031.

[34] S. R. Anton and D. J. Inman, "Vibration energy harvesting for unmanned aerial vehicles," *Proceedings SPIE 6928, Active and Passive Smart Structures and Integrated Systems 2008*, vol. 6928, 2008, https://doi.org/10.1117/12.774990.

[35] P. M. G. B. Asdaque, R. K. Behera, and J. H. Shaik, "Vibration analysis of multi-disk multi-profiled shaft-rotor systems," *Applied Mechanics and Materials*, vol. 612, pp. 17–22, 2014, https://doi.org/10.4028/www.scientific.net/AMM.612.17.

[36] A. M. Formalskii, "Unstable mechanical objects: motion control, stabilization," *Universal Journal of Mechanical Engineering*, vol. 5, no. 5, pp. 150–169, 2017, https://doi.org/10.13189/ujme.2017.050503.

[37] R. Guo, S. Han, M.-J. Wang, and C. Cao, "Electric motor-based crankshaft stop position control to suppress range extender start vibration in electric vehicle," *Journal of Low Frequency Noise, Vibration and Active Control*, vol. 37, no. 3, pp. 422–442, 2018, https://doi.org/10.1177/0263092317711598.

[38] A. Hati, C. Nelson, and D. Howe, "Vibration-induced PM noise in oscillators and its suppression," *Aerial vehicles*, pp. 259–286, 2009, https://doi.org/10.5772/6476.

[39] H. Mingchao, L. Haoyan, Z. Pengbo, S. Guoliang and J. Shuqiang, "Impact of Vibrating Antenna on the Performance of M-QAM Wireless Communication System," *2020 IEEE 3rd International Conference on Computer and Communication Engineering Technology (CCET)*, pp. 278-283, 2020, https://doi.org/10.1109/CCET50901.2020.9213139.

[40] S.-H. Kim, Z. W. Geem, and G.-T. Han, "Hyperparameter optimization method based on harmony search algorithm to improve performance of 1D CNN human respiration pattern recognition system," *Sensors*, vol. 20, no. 13, p. 3697, 2020, https://doi.org/10.3390/s20133697.

[41] N. Srivastava, G. Hinton, A. Krizhevsky, I. Sutskever, and R. Salakhutdinov, "Dropout: a simple way to prevent neural networks from overfitting," *The journal of machine learning research*, vol. 15, no. 1, pp. 1929-1958, 2014, https://www.jmlr.org/papers/volume15/srivastava14a/srivastava14a.pdf?utm_content=buffer79b43&utm_medium=social&utm_source=twitter.com&utm_campaign=buffer.

[42] S. Kiranyaz, T. Ince, R. Hamila and M. Gabbouj, "Convolutional Neural Networks for patient-specific ECG classification," *2015 37th Annual International Conference of the IEEE Engineering in Medicine and Biology Society (EMBC)*, pp. 2608-2611, 2015, https://doi.org/10.1109/EMBC.2015.7318926.

[43] S. Kiranyaz, T. Ince, and M. Gabbouj, "Personalized monitoring and advance warning system for cardiac arrhythmias," *Scientific reports*, vol. 7, no. 1, p. 9270, 2017, https://doi.org/10.1038/s41598-017-09544-z.

[44] O. Avci, O. Abdeljaber, S. Kiranyaz, M. Hussein, and D. J. Inman, "Wireless and real-time structural damage detection: A novel decentralized method for wireless sensor networks," *Journal of Sound and Vibration*, vol. 424, pp. 158-172, 2018, https://doi.org/10.1016/j.jsv.2018.03.008.

[45] O. Avci, O. Abdeljaber, S. Kiranyaz, and D. Inman, "Structural damage detection in real time: implementation of 1D convolutional neural networks for SHM applications," *Structural Health Monitoring & Damage Detection*, vol. 7, pp. 49-54, 2017, https://doi.org/10.1007/978-3-319-54109-9_6.

[46] O. Abdeljaber, O. Avci, S. Kiranyaz, M. Gabbouj, and D. J. Inman, "Real-time vibration-based structural damage detection using one-dimensional convolutional neural networks," *Journal of Sound and Vibration*, vol. 388, pp. 154-170, 2017, https://doi.org/10.1016/j.jsv.2016.10.043.

[47] O. Avci, O. Abdeljaber, S. Kiranyaz, B. Boashash, H. Sodano, and D. J. Inman, "Efficiency validation of one dimensional convolutional neural networks for structural damage detection using a SHM benchmark data," *25th International Congress on Sound and Vibration 2018*, pp. 4600-4607, 2018, https://www.diva-portal.org/smash/record.jsf?pid=diva2%3A1362683&dswid=7541.

[48] O. Abdeljaber, O. Avci, M. S. Kiranyaz, B. Boashash, H. Sodano, and D. J. Inman, "1-D CNNs for structural damage detection: Verification on a structural health monitoring benchmark data," *Neurocomputing*, vol. 275, pp. 1308-1317, 2018, https://doi.org/10.1016/j.neucom.2017.09.069.

[49] T. Ince, S. Kiranyaz, L. Eren, M. Askar and M. Gabbouj, "Real-Time Motor Fault Detection by 1-D Convolutional Neural Networks," *IEEE Transactions on Industrial Electronics*, vol. 63, no. 11, pp. 7067-7075, 2016, https://doi.org/10.1109/TIE.2016.2582729.

[50] S. Kiranyaz, A. Gastli, L. Ben-Brahim, N. Al-Emadi and M. Gabbouj, "Real-Time Fault Detection and Identification for MMC Using 1-D Convolutional Neural Networks," *IEEE Transactions on Industrial Electronics*, vol. 66, no. 11, pp. 8760-8771, 2019, https://doi.org/10.1109/TIE.2018.2833045.

[51] O. Abdeljaber, S. Sassi, O. Avci, S. Kiranyaz, A. A. Ibrahim and M. Gabbouj, "Fault Detection and Severity Identification of Ball Bearings by Online Condition Monitoring," *IEEE Transactions on Industrial Electronics*, vol. 66, no. 10, pp. 8136-8147, 2019, https://doi.org/10.1109/TIE.2018.2886789.

[52] J. Menčík, "Monte Carlo simulation method," *Concise Reliability for Engineers*, 2016, https://doi.org/10.5772/62369.

[53] L. A. Al-Haddada, A. A. Jaberb, P. Neranonc, and S. A. Al-Haddadd, "Investigation of Frequency-Domain-Based Vibration Signal Analysis for UAV Unbalance Fault Classification," *Engineering and Technology Journal*, vol. 41, no. 7, pp. 915-923, 2023, https://doi.org/10.30684/etj.2023.137412.1348.

[54] R. L. Harrison, "Introduction to monte carlo simulation," *AIP conference proceedings*, vol. 1204, no. 1, pp. 17-21, 2010, https://doi.org/10.1063/1.3295638.

[55] R. J. Cintra, S. Duffner, C. Garcia and A. Leite, "Low-Complexity Approximate Convolutional Neural Networks," *IEEE Transactions on Neural Networks and Learning Systems*, vol. 29, no. 12, pp. 5981-5992, 2018, https://doi.org/10.1109/TNNLS.2018.2815435.

[56] N. Rusk, "Deep learning," *Nature Methods*, vol. 13, no. 1, p. 35, 2016, https://doi.org/10.1038/nmeth.3707.

[57] R. J. Cintra, S. Duffner, C. Garcia and A. Leite, "Low-Complexity Approximate Convolutional Neural Networks," *IEEE Transactions on Neural Networks and Learning Systems*, vol. 29, no. 12, pp. 5981-5992, 2018, https://doi.org/10.1109/TNNLS.2018.2815435.

[58] Z. Zhang, P. Cui and W. Zhu, "Deep Learning on Graphs: A Survey," *IEEE Transactions on Knowledge and Data Engineering*, vol. 34, no. 1, pp. 249-270, 2022, https://doi.org/10.1109/TKDE.2020.2981333.

[59] W. H. L. Pinaya, S. Vieira, R. Garcia-Dias, A. Mechelli, "Convolutional neural networks," *Machine learning*, pp. 173-191, 2020, https://doi.org/10.1016/B978-0-12-815739-8.00010-9.

[60] Z. Li, F. Liu, W. Yang, S. Peng and J. Zhou, "A Survey of Convolutional Neural Networks: Analysis, Applications, and Prospects," *IEEE Transactions on Neural Networks and Learning Systems*, vol. 33, no. 12, pp. 6999-7019, 2022, https://doi.org/10.1109/TNNLS.2021.3084827.

[61] N. Bačanin Džakula, "Convolutional neural network layers and architectures," *Sinteza 2019-International Scientific Conference on Information Technology and Data Related Research*, pp. 445–451, 2019, https://doi.org/10.15308/Sinteza-2019-445-451.